ing coefficients (*26*) of the peptides AcYKFLG-OH (90) and AcYIFLG-OH (10) with the corresponding oligocarbamates AcY^{c}K^{c}F^{c}L^{c}G-OH (0.5) and AcY^{c}I^{c}F^{c}L^{c}G-OH (0.4) revealed the latter to be significantly more hydrophobic. Moreover, oligocarbamates were significantly more resistant to proteolytic degradation than peptides. Treatment of the peptides AcYKFLG-OH and AcYIFLG-OH with trypsin or porcine pepsin, respectively, resulted in complete degradation within 20 min whereas the corresponding oligocarbamates showed no appreciable degradation after 150 min (*27*). These characteristics of oligocarbamates may be reflected in enhanced pharmacokinetic properties relative to oligopeptides. The structural and pharmacological properties of oligocarbamates and other polymers (such as substituted ureas and sulfones) may not only provide new tools for medicinal chemists buy may also provide new opportunities to construct two- and three-dimensional biopolymers with novel properties.

REFERENCES AND NOTES

1. R. B. Merrifield, *J. Am. Chem. Soc.* **85**, 2149 (1963); *Science* **232**, 341 (1986).
2. M. Hagihara, N. J. Anthony, T. J. Stout, J. Clardy, S. L. Schreiber, *J. Am. Chem. Soc.* **114**, 6568 (1992); R. J. Simon *et al.*, *Proc. Natl. Acad. Sci. U.S.A.* **89**, 9367 (1992).
3. A. M. Bray, N. J. Maeji, H. M. Geysen, *Tetrahedron Lett.* **31**, 5811 (1990).
4. S. P. A. Fodor *et al.*, *Science* **251**, 767 (1991).
5. R. A. Houghten *et al.*, *Nature* **354**, 84 (1991).
6. K. S. Lam *et al.*, *ibid.*, p. 82 (1991).
7. J. Blake and L. Litzi-Davis, *Bioconjugate Chem.* **3**, 510 (1992).
8. M. C. Needels *et al.*, *Proc. Natl. Acad. Sci. U.S.A.*, in press.
9. A. Eschenmoser and M. Dobler, *Helv. Chim. Acta.* **75**, 218 (1992); A. B. Smith III *et al.*, *J. Am. Chem. Soc.* **114**, 10672 (1992).
10. D. D. Weller, D. T. Daly, W. K. Olson, J. E. Summerton, *J. Org. Chem.* **56**, 6000 (1991); J. M. Coull, D. V. Carlson, H. L. Weith, *Tetrahedron Lett.* **28**, 745 (1987); W. S. Mungall and J. K. Kaiser, *J. Org. Chem.* **42**, 703 (1977); B. R. Baker, P. M. Tanna, G. D. F. Jackson, *J. Pharm. Sci.* **54**, 987 (1965).
11. J. C. Hanvey *et al.*, *Science* **258**, 1481 (1992); E. Uhlmann and A. Peyman, *Chem. Rev.* **90**, 543 (1990).
12. Reduction with this method yields optically pure amino alcohols: J. Nikawa and T. Shiba, *Chem. Lett.* **1979**, 981 (1979). Single diastereomers were observed by ^{1}H nuclear magnetic resonance after carbamate couplings.
13. A. Patchornik, B. Amit, R. B. Woodward, *J. Am. Chem. Soc.* **92**, 6333 (1970).
14. L. A. Carpino and G. Y. Han, *J. Org. Chem.* **37**, 3404 (1972).
15. S.-S. Wang, *J. Am. Chem. Soc.* **95**, 1328 (1973); G. Lu, S. Mojsov, J. P. Tam, R. B. Merrifield, *J. Org. Chem.* **46**, 3433 (1981).
16. H. Rink, *Tetrahedron Lett.* **28**, 3787 (1987).
17. D. S. King, C. G. Fields and G. B. Fields, *Int. J. Peptide Protein Res.* **36**, 255 (1990).
18. E. Kaiser, R. L. Colescott, C. D. Bossinger, P. I. Cook, *Anal. Biochem.* **34**, 595 (1970); V. K. Sarin, S. B. H. Kent, J. P. Tam, R. B. Merrifield, *ibid.* **117**, 147 (1981).
19. Oligocarbamates were purified by preparative reversed-phase HPLC with a Whatman M-20 10/50 Partisil ODS-10 column at a flow rate of 8.0 ml/min and a linear gradient of 90%A/10%B to 0%A/100%B over 120 min; A, 0.1% trifluoroacetic acid (TFA)/H_2O; and B, 0.08% TFA/CH_3CN, 260 nm detection wavelength; followed by lyophilization.
20. Oligocarbamate sequences are designated by the names of the corresponding amino acids with a superscript c to indicate a carbamate bond. For example, the oligocarbamate where R_1 = *p*-hydroxybenzyl, R_2 = 1-aminobutyl, R_3 = benzyl, and R_4 = 2-methylpropyl is designated Ac-Y^{c}K^{c}-F^{c}L^{c}-NH_2, where Ac is acetyl. Abbreviations for the amino acid residues are: A, Ala; C, Cys; D, Asp; E, Glu; F, Phe; G, Gly; H, His; I, Ile; K, Lys; L, Leu; M, Met; N, Asn; P, Pro; Q, Gln; R, Arg; S, Ser; T, Thr; V, Val; W, Trp; and Y, Tyr.
21. Antibody was used directly from hybridoma cell culture supernatants: S. J. Pollack, P. Hsiun, P. G. Schultz, *J. Am. Chem. Soc.* **111**, 5961 (1989).
22. Ligands of various concentrations in 50 mM tris-saline buffer, pH 7.4, were preincubated with antibody 20D6.3 (~1 μg/ml) for 1 hour at 37°C, transferred to Ac-Y^{c}K^{c}F^{c}L^{c}G-BSA–coated ELISA plates (5 μg/ml) for 2 hours at 37°C, and developed with goat-α-mouse alkaline phosphatase conjugate for 1 hour at 37°C followed by addition of *p*-nitrophenyl phosphate.
23. The NHS ester of the nitrophenylsulfenyl-protected hapten was coupled to keyhole limpet hemocyanin, and the resulting conjugate was deprotected by treatment with sodium dithionite to give a hapten to carrier density of 4.
24. The ligand AcY^{c}F^{c}L^{c}-OH (synthesized on glass via FMOC chemistry) also gave a low fluorescence signal when assayed against 20D6.3.
25. M. Oki and H. Nakanishi, *Bull. Chem. Soc. Jpn.* **44**, 3148 (1971); S. van der Werf, R. Olijnsma, J. B. F. N. Engberts, *Tetrahedron Lett.* 689 (1967); C. M. Lee and W. D. Kumler, *J. Am. Chem. Soc.* **83**, 4596 (1961).
26. Water:octanol partitioning coefficients were determined as described [J.-L. Fauchère and V. Pliska, *Eur. J. Med. Chem.* **18**, 369 (1983)] by using 1-octanol and 10 mM phosphate buffer, pH 7.4 [final dimethylsulfoxide (DMSO) concentration 1%]. Concentration of ligands was determined spectrophotometrically by absorbance at 280 nm.
27. Trypsin (670 nM) was incubated at room temperature with either peptide substrate AcYKFLG-OH (630 μM) or carbamate ligand AcY^{c}K^{c}F^{c}L^{c}G-OH (420 μM) in tris-saline buffer, pH 7.4, containing 1% DMSO and 1% acetonitrile. Similarly, porcine pepsin (0.1 M formate buffer, pH 3.1, 1.1 μM) was incubated with peptide substrate AcYIFLG-OH (440 μM) or oligocarbamate AcY^{c}I^{c}F^{c}L^{c}G-OH (390 μM). Degradation of substrates was monitored by reversed-phase analytical HPLC.
28. This work was supported by the director, Office of Energy Research, Office of Biological & Environmental Research, General Life Sciences Division, of the U.S. Department of Energy under contract DE-AC03-76SF00098, by the Office of Naval Research (grant N00014-93-1-0380) and by a grant from the Lucille P. Markey Charitable Trust. E.J.M. was supported by the National Institutes of Health for a postdoctoral fellowship (grant 1 F32 GM14681). We also acknowledge Applied Biosystems for assistance in adapting oligocarbamate synthesis to the ABI automated synthesizer and J. Ellman and D. King for helpful discussions.

15 April 1993; accepted 23 July 1993

Discovery of Vapor Deposits in the Lunar Regolith

Lindsay P. Keller* and David S. McKay

Lunar soils contain micrometer-sized mineral grains surrounded by thin amorphous rims. Similar features have been produced by exposure of pristine grains to a simulated solar wind, leading to the widespread belief that the amorphous rims result from radiation damage. Electron microscopy studies show, however, that the amorphous rims are compositionally distinct from their hosts and consist largely of vapor-deposited material generated by micrometeorite impacts into the lunar regolith. Vapor deposits slow the lunar erosion rate by solar wind sputtering, influence the optical properties of the lunar regolith, and may account for the presence of sodium and potassium in the lunar atmosphere.

One of the expectations during the Apollo program was that the mineral grains in lunar soils would provide an opportunity to monitor the activity of the ancient sun and the properties of the solar wind as a function of time. However, it was soon realized that determination of the exposure history of individual grains was complicated by regolith processes, namely, meteoroid impact "gardening" on the lunar surface. Nevertheless, some workers tried to deduce the characteristics of the ancient solar wind from data acquired primarily from high-voltage transmission electron microscope (TEM) studies of the fine-grained fractions of lunar soils. It was discovered that many of the mineral grains in the submicrometer size range are surrounded by thin amorphous layers (*1*) that, it was demonstrated, could be produced by exposing mineral grains to a high flux of low-energy ions in the laboratory. This result suggested that the interaction of the solar wind with crystalline grains could produce the thin layer, where the crystallinity of the host grain was destroyed by implantation of solar wind ions (*2*–*4*). The concept that the amorphous rims are a result of radiation damage has been widely cited and is firmly ensconced in the literature. Our examination of the amorphous rims and their host grains shows, however, that most, if not all, of the amorphous rims formed primarily by the

---

Solar System Exploration Division, NASA Johnson Space Center, Houston, TX 77058.

*Present address: Lockheed, C23, 2400 NASA Road 1, Houston, TX 77258.

deposition of impact-generated vapors and that contributions from solar wind radiation damage are at most a minor effect.

We used a TEM equipped with an energy-dispersive x-ray (EDX) spectrometer to analyze thin sections of fine-grained lunar soils (5). We analyzed nearly 80 amorphous rims and their mineral hosts from soil samples 10084, 61181, and 78221 from the Apollo 11, 16, and 17 landing sites, respectively. These soils have had long surface exposure and would thus be expected to have thick rims. The mineral grains from these mature soils typically contain a high density of solar flare tracks ($\sim 10^{10}$ to 10^{11} tracks per square centimeter), which also indicates long periods of exposure. We observed amorphous rims on a variety of minerals, including anorthite, augite, orthopyroxene, olivine, and cristobalite (Fig. 1), from mature soils. Rims were not observed on ilmenite grains primarily because there are very few micrometer-sized and smaller ilmenite grains in the soils we studied. Rim thicknesses (measured in thin section) ranged from 10 to 200 nm but averaged 50 to 60 nm. Over 50% of the analyzed amorphous rims contain nanometer-sized crystalline inclusions. Electron diffraction of the larger inclusions showed that Fe metal is the most abundant inclusion type. Two amorphous rims on anorthite grains from 10084 contained submicroscopic grains of ilmenite. In extreme cases, a stratigraphy is observed within the amorphous rim, suggesting that multiple events of vapor deposition occurred (Fig. 2).

Every rim analyzed showed compositional differences from the host grain, ranging from slight increases in Fe and Mg on some anorthite grains to very dramatic changes such as a basaltic-composition rim on cristobalite (SiO_2). Whereas individual rim compositions are variable, the average rim composition approximates the bulk soil composition, with some notable exceptions (Fig. 3): In all three soils, the average rim composition is markedly enriched in S and is more Si-rich than the bulk soil. The finest fractions of lunar soils are also known to be enriched in S, which is thought to be present on the grain surfaces (6, 7). Furthermore, the average rim is depleted in Mg, Ca, Ti, and in some soils, Al, compared with the bulk soil.

The observed pattern of enrichment in the more volatile elements and depletions in refractory elements is most consistent with rim formation by vapor deposition. Studies of the vaporization process and the chemical fractionations that occur during the evaporation of lunar basalts or basaltic analogs (8, 9) have shown that during evaporation, volatile elements (mainly Na, K, Si, and Fe) are preferentially vaporized relative to the more refractory elements (such as Ca, Al, and Ti), which tend to be concentrated in the residual material. These chemical fractionations are known from lunar impact glasses (*10*) and are dramatically illustrated in the finest grain sizes of lunar soils, for which the high surface area contributes to extreme fractionations (*11*). The TEM studies of the finest fractions of lunar soils show that the compositions of the submicrometer glasses are dominated by fractionated compositions, either refractory-rich or volatile-rich glasses (*11*). The volatile-rich glasses are markedly depleted in refractory elements such as Ca, Al, and Ti; strongly enriched in Si and Fe (and to a lesser degree, Na, K, and S); and are believed to have formed as condensates of impact-generated vapors (*11*).

If the amorphous rims form by the deposition of vapors as we propose, then we would also expect to see marked enrichments in Na, K, and Fe. The fate of the highly volatile elements (like Na and K) is, however, ambiguous. Although typical lunar soils have a low abundance of the alkali elements, we do not observe enrichments of Na or K in the amorphous coatings. Alkali elements are known to be mobile during analysis in the electron microscope, so that the lack of an alkali enrichment may be an artifact of the analysis procedure. An interesting alternative is that Na and K do not recondense as efficiently as the other less-volatile elements and thus give rise to the Na and K that occurs in the lunar atmosphere (*12*). The lack of a strong Fe enrichment in the rims may result from the mechanism of vapor generation and deposition. Zoning of vapor deposits has been documented (*13*), and we propose that Fe condenses as discrete metallic droplets that are partly incorporated into the amorphous rims, and the remainder are added to the population of submicroscopic metal grains in lunar soils.

Strong arguments have been made for sputtered-ion deposition as the major process in the production of surface deposits, particularly surficial Fe enrichments (*14*). However, the enrichments we observed are not consistent with this model because sputtering is generally a strong function of atomic number (deposits formed by sputter deposition should be enriched in heavier elements). Our data indicate that sputtered-ion deposition can only form a minor component of the rims and that deposition of impact-generated vapors is by far the dominant process. This result has important implications for the long-term erosion rate on the lunar surface because the effective sputtering rates will be largely overwhelmed by the addition of vapor-deposited materials. A sputtering rate of ~0.05 nm/year was deduced (*4*) on the assumption that the amorphous rims result from solar

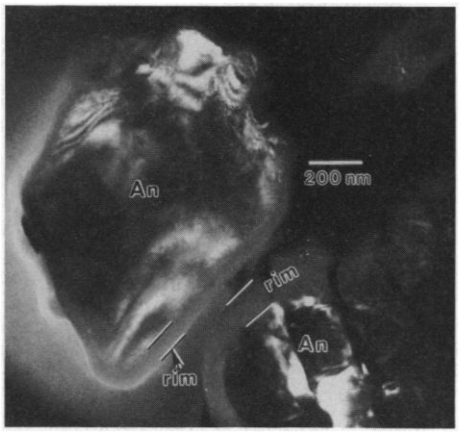

Fig. 1. Dark-field TEM image of anorthite (An) grains with amorphous rims from soil sample 61181. The rim on the grain in the lower right corner of the figure contains small (~5 nm) bright inclusions that are probably Fe metal.

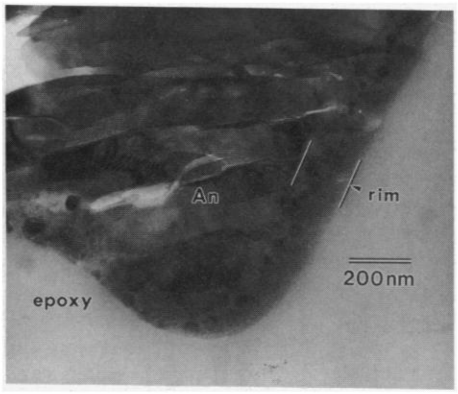

Fig. 2. Bright-field TEM image of a thick amorphous rim on an anorthite grain from soil sample 61181. The dark inclusions in the rim are mostly Fe metal with a few FeS grains. The Fe grains are concentrated in layers within the rim and may indicate successive episodes of vapor deposition.

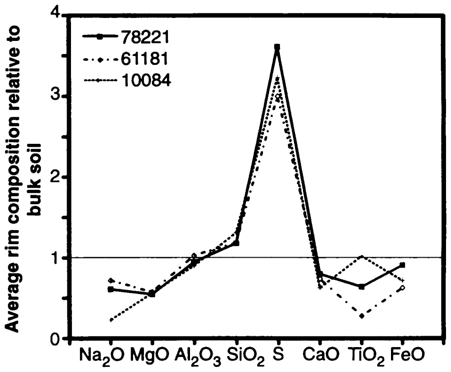

Fig. 3. Average composition of amorphous rims on soil grains from three lunar soils ratioed to the bulk composition of the <20-μm size fraction of the local soil in each case. Ratios >1 indicate enrichments over the bulk soil.

wind radiation damage, which is over two orders of magnitude greater than estimates based on the buildup of solar wind–implanted species, such as Ar and He (*15*). Our data support the conclusions of Kerridge and Kaplan (*16*), who suggested that the effective sputtering rate on the lunar surface is slowed by the simultaneous accumulation of impact-generated vapors.

If amorphous rims result from radiation damage (*1–4*), then the rims should be compositionally the same as their hosts. However, the compositional differences observed in this study, combined with the distribution of Fe particles in the rims, indicates that solar wind radiation damage is not the major mechanism for the formation of amorphous rims. Solar wind damage can have, at most, a minor effect. It has been suggested that the ancient solar wind was not as active as the contemporary wind, on the basis of the thickness of the amorphous rims and assumptions regarding the exposure history of individual soil grains on the lunar surface (*4*); this conclusion is not valid.

Hapke *et al.* (*14*) showed that experimental vapor coatings produced by vapor deposition and sputtered ion deposition are dark and have optical properties that resemble those of the lunar fines. Hapke also showed that sputtering of lunar fines produces the requisite darkening. In all these cases, it seems that the most important ingredient is the presence of submicroscopic Fe metal grains, which are strong absorbers of visible wavelengths. The presence of fine-grained Fe metal in the amorphous rims could also contribute to the darkening process, but it is not yet known if there is a sufficient concentration of Fe particles to have a significant effect.

Theoretical work indicates that considerable amounts of vapor should be produced during micrometeorite impacts into the lunar regolith and that much of the vapor must recondense onto nearby soil grains (*17, 18*). However, questions remain regarding the fate of impact-generated vapors because no petrographically distinct vapor-deposited material had been identified in lunar soils. Despite a considerable body of evidence that the surfaces of lunar fines are enriched in some elements relative to the bulk soil (*19–22*), there has been no consensus on the degree of enrichment or on the mechanism responsible for the surface enrichments. Our study shows that vapor deposits are present in the lunar regolith as thin amorphous rims on soil grains. The main characteristics of these condensates are an enrichment in volatile elements (particularly Si and S), a marked depletion in refractory elements, and Fe in the form of metallic particles on the order of nanometers in size. Contributions to these amorphous coatings by sputtered iron deposition and radiation damage are probably of minor importance relative to the contribution of direct condensation of impact-generated vapors.

REFERENCES AND NOTES

1. J. C. Dran *et al.*, *Earth Planet. Sci. Lett.* **9**, 391 (1970).
2. J. Bibring *et al.*, *Science* **175**, 753 (1972).
3. M. Maurette and P. B. Price, *ibid.* **187**, 121 (1975).
4. J. Borg *et al.*, in *The Ancient Sun: Fossil Record in the Earth, Moon, and Meteorites*, R. O. Pepin, J. A. Eddy, R. B. Merrill, Eds. (Pergamon, New York, 1980), p. 431.
5. Aliquots of the <20-μm size fraction of each soil were embedded in low-viscosity epoxy, and thin sections ~100 nm thick were prepared by diamond knife ultramicrotomy. The EDX analyses were collected so that counting statistics errors for major elements were <1%; relative errors associated with the determination of experimental *k* factors are <5%. Microtome thin sections of the soils were analyzed using a JEOL 2000FX TEM equipped with a LINK EDX spectrometer. Probe sizes were typically 30 to 40 nm, less than the apparent thickness of the amorphous rims. Multiple analyses of individual rims fall within the analytical uncertainties of the EDX technique.
6. C. E. Rees and H. G. Thode, *Proc. Lunar Planet. Sci. Conf.* **5**, 1963 (1974).
7. J. D. Cripe and C. B. Moore, *ibid.* **7**, 469 (1976).
8. G. DeMaria *et al.*, *ibid.* **2**, 1367 (1971).
9. A. V. Ivanov and K. P. Florensky, *ibid.* **6**, 1341 (1975).
10. M. T. Naney *et al.*, *ibid.* **7**, 155 (1976).
11. L. P. Keller and D. S. McKay, *Lunar Planet. Sci.* **XXII**, 137 (1992).
12. A. E. Potter and T. H. Morgan, *Science* **241**, 675 (1988).
13. O. I. Yakovlev *et al.*, *Geokhimiya* **12**, 1698 (1988).
14. B. Hapke *et al.*, *Moon* **13**, 339 (1975).
15. J. F. Kerridge, *Lunar Planet. Sci. Conf.* **XXI**, 301 (1991).
16. ——— and I. R. Kaplan, *ibid.* **9**, 1687 (1978).
17. H. A. Zook, *ibid.* **6**, 1653 (1975).
18. M. J. Cintala, *J. Geophys. Res.* **97**, 947 (1992).
19. B. Hapke *et al.*, in *Proceedings of the Apollo 11 Lunar Science Conference*, A. A. Levinson, Ed. (Pergamon, New York, 1970), p. 2199.
20. T. Gold *et al.*, *Proc. Lunar Planet. Sci. Conf.* **7**, 901 (1976).
21. R. M. Housley and R. W. Grant, *ibid.*, p. 881.
22. E. Zinner *et al.*, *ibid.* **9**, 1667 (1978).

23. This work supported by NASA RTOP 152-17-40-21. We thank H. Zook for a review of an early version of the manuscript.

22 April 1993; accepted 2 July 1993

Lattice Effect of Strong Electron Correlation: Implication for Ferroelectricity and Superconductivity

T. Egami,* S. Ishihara, M. Tachiki

Much theoretical work has been devoted to understanding the role of strong electron correlations in high-temperature superconductivity mainly through magnetic interactions, but the possible role of electron correlation in ferroelectricity of metal oxides has not received attention. Diagonalization of a simple many-body, tight-binding Hamiltonian shows that the electron-lattice interaction is dramatically enhanced in some cases by strong electron correlation because of deformation-induced charge transfer. This effect may be closely related to ferroelectricity and superconductivity in transition metal oxides.

High-temperature superconductors are doped Mott insulators, such as $La_{2-x}Sr_xCuO_4$. In the Mott insulator, conduction is inhibited by strong electron-electron correlation, which does not allow two carriers to be on the same lattice site. One consequence of strong electron correlation is the spin polarization of an atom, and much theoretical attention in high-temperature superconductivity has focused on the effect of magnetic interactions (*1, 2*). In comparison, there has been relatively little discussion of the effect of electron correlation on the electron-lattice interaction. Even less has been written about the possible role of electron correlation in ferroelectricity, although superconducting oxides are close in composition and structure to ferroelectric oxides and there is a possible connection (*3, 4*). We suggest that strong electron correlation can have a significant effect on the electron-lattice interaction with some drastic consequences in certain situations, and this could have profound implications for the mechanism of ferroelectricity and possibly of high-temperature superconductivity.

The origin of ferroelectricity in transition metal oxides such as $BaTiO_3$ is usually discussed in terms of ionic displacements and the internal Lorentz field produced by the polarization. However, the inadequacy of such a simple view has been known for a long time (*5*), and the need to take the covalency of the bond into account has been advocated. A recent local density approximation (LDA)–linearized augmented plane wave (LAPW) calculation on $BaTiO_3$ (*6*) demonstrates the importance of covalency in ferroelectric po-

---

Institute for Materials Research, Tohoku University, Sendai 980, Japan.

*Also in the Department of Materials Science and Engineering and the Laboratory for Research on the Structure of Matter, University of Pennsylvania, Philadelphia, PA 19104–6272.